Mesoporous Silica Colloids: Wetting, Surface Diffusion, and Cationic Surfactant Adsorption

Elise Azar, Christophe Blanc, Ahmad Mehdi, Maurizio Nobili, Antonio Stocco

HAL Id: hal-02341812
https://hal.science/hal-02341812

Submitted on 31 Oct 2019

Mesoporous Silica Colloids: Wetting, Surface Diffusion and Cationic Surfactant Adsorption

Elise Azar,[a,b] Christophe Blanc,[a] Ahmad Mehdi,[c] Maurizio Nobili[a] and Antonio Stocco[*a,b]

[a]Laboratoire Charles Coulomb (L2C), University of Montpellier, CNRS, Montpellier, France

[b]Institut Charles Sadron (ICS), University of Strasbourg, CNRS, Strasbourg, France

[c]Institut Charles Gerhardt (ICGM), University of Montpellier, CNRS, ENSCM, Montpellier, France

[*]stocco@unistra.fr, Telephone: +33 (0)388414113, Fax: +33 (0)388414099

ABSTRACT

We have investigated the wetting and surface diffusion of mesoporous colloidal silica particles at the water surface; and the adsorption of cationic cetyltrimethylammonium (CTA^+) surfactant on these particles. Porous silica colloids diffuse at the surface of water and in the volume, interacting with cationic surfactants that can adsorb inside the pores of the particles. We observed that surfactant adsorption on mesoporous silica depends dramatically not only on the particle pore size but also on specific counterion effects. We measured striking differences both on a macroscopic property of the interface, i.e. surface tension, and also at a single particle level by evaluating the translational diffusion of partially wetted particles at the fluid interface. We varied the pore size from 2 to 7 nm and explored the effects of ions owing different hydration number and kosmotropic/chaotropic character. At concentrations lower than the critical micellar concentration, we evidence that cationic surfactants adsorb on silica as surface micelles and surfactant adsorption inside the pores occurs only if the pore diameter is larger than the size of surface micelles. With a view to understand the surprising different adsorption behavior of CTA^+OH^- and CTA^+Br^- on porous silica particles, we investigated the effect of counterions on the surfactant adsorption on porous silica colloids by tuning the pH and the counterion properties.

INTRODUCTION

Cationic surfactants are widely used in many industrial and fundamental research fields ranging from cosmetics, fabrics, nanoparticles synthesis, DNA folding, self-assembly and mesoporous material fabrication.[1,2] Besides these applications, the fate of cationic surfactants and the resulting waste in water is an important issue, since cationic surfactant contamination of water represents an real environmental problem.[3] Current methods to remove surfactants from water involve the use of organophilic clays, flocculants or carbon beds.[4–8] In many separation methods, surfactant removal by adsorption onto solid substrates is required. Hence, both large surface areas and an effective attraction between the surfactant and the solid are necessary to drive soluble surfactants adsorption on the solid boundaries.

Adsorption of cationic surfactants on planar solid surfaces has been investigated for several surfactant-substrate systems. For cetyltrimethylammonium (CTA^+) surfactants on silica surfaces, different adsorption regimes are found as a function of the surfactant concentration, surface charge and

39 hydrophobic interaction.[9,10] At low concentrations, surfactant may adsorb onto the silica surface as a
40 monolayer, as defective bilayers or as surface micelles.[11,12] These micellar structures are flattened by the
41 surface and possess a thickness of 3.5 nm and a lateral size of 9 nm.[10] Upon increasing the concentration,
42 bilayers may form due to the interaction between the hydrophobic chains. It is important to notice that the
43 interfacial self-assembled structures usually appear at a concentration lower than the usual critical
44 micellar concentration (CMC) in the volume.[11] For CTA$^+$ surfactants at concentrations C lower but close
45 to CMC, surface excess concentrations Γ between ≈ 1 and ≈ 2 mg/m^2 have been reported.[11,13–15]

46 As pointed out before, solid substrates with large specific areas are required for adsorption in order to
47 separate surfactants from clean water. In this context, porous particles are ideal candidates given the large
48 surface/volume ratio, which can be tuned by the pore size and volume fraction.[16,17] However, adsorption
49 inside a pore strongly differs from the adsorption on a planar interface. Pore size and morphology affect
50 the adsorption process, which depends on differences in pressure and physicochemical properties inside
51 and outside the pores.[18]

52 Non-ionic surfactants adsorption onto mesoporous silica particles has been widely investigated by
53 Findenegg and coworkers.[19–22] Bilayers formation and other structures inside the pores has been reported.
54 Very few experimental investigations can be found in the literature for the adsorption of cationic
55 surfactants onto mesoporous silica. A small angle neutron scattering investigation reported some
56 preliminary experiments for 8 nm pore size mesoporous silica at pH=9 where an increase of cationic
57 surfactant adsorption occurs if the ionic strength is increased.[23] Cationic surfactant interacting with silica
58 nanoparticles have been also recently investigated.[1,24–26]

59 Here, we have investigated the wetting and diffusion of porous silica colloids, and the adsorption of
60 cationic surfactants on porous colloidal particles. Porous colloids of different pore sizes are deposited
61 both in the bulk and at the interface. By varying pore size, surfactant concentration and investigating
62 counterion effects we aim at controlling CTA$^+$ cationic surfactant adsorption. These results could be used
63 in order to develop a strategy to clean the surface and the volume of water with micron sized particles,
64 which are small enough to perform Brownian motion and rapidly diffuse at the interface (and in the
65 volume) but also large enough to slowly sediment. These porous colloids may be ideal candidates for an
66 efficient removal of surfactants at low concentrations and present the advantage to be easily removed
67 after decontamination by sedimentation or flotation. Note that larger particles are difficult to adsorb at the
68 interface and may sediment very fast; whilst nanoparticles may remain dispersed in water due to the
69 strong Brownian motion and cannot be separated by gravity or adsorption on bubbles as in flotation.

70

71

MATERIALS AND METHODS

73 *Materials.* All chemicals, except for the in-house synthetized colloids, were purchased from Sigma
74 Aldrich and used without further purification. Two surfactants were investigated:
75 cetyltrimethylammonium bromide CTA$^+$Br$^-$ (CAS 57-09-0, molecular weight M_w = 364.45 g/mol) and
76 cetyltrimethylammonium hydroxide CTA$^+$OH$^-$ (10 wt.% in H$_2$O, CAS 505-86-2, M_w = 301.55 g/mol).
77 Three different batches of porous silica particles were also employed. The first two consist of spherical
78 mesoporous silica colloids (CAS 7631-86-9) with an average radius $\bar{R}$ = 1.23 $\pm$ 0.10 µm (measured by
79 scanning electron microscopy, SEM) and nominal pore diameter d = 2 nm and d = 4 nm and a specific
80 area S_A = 1000 $\pm$ 100 m^2/g for d = 2 nm and S_A = 350 $\pm$ 50 m^2/g for d = 4 nm. A third batch of non-
81 spherical mesoporous silica particles was synthetized in the laboratory. These last particles are currently

82   called Santa Barbara amorphous-15 silica (SBA-15). The average pore diameter is larger than the
83   previous ones: $d = 7$ nm measured by volumetric nitrogen sorption isotherms. Stable particle dispersions
84   were obtained by sonication of 1.2 mg/mL dispersions in an ultrasound bath for one hour. We measured
85   the Feret diameter[27] of these particles by scanning electron microscopy, which leads to an equivalent
86   radius $\bar{R} = 1.96 \pm 0.97$ μm (*i.e.* half of the Feret diameter). The pores are about a micron long and
87   connected via mesoporous walls. A total specific area of 750 ± 50 m^2/g was evaluated by Brunauer-
88   Emmett-Teller (BET) method. Pore size distributions were determined by the (Barrett, Joyner, Halend)
89   BJH method.[28] Mesoporous walls contribute significantly to the total specific area in terms of
90   microporosity (size < 1-2 nm). We evaluate a total specific area $S_A = 225 \pm 25$ m^2/g for the $d = 7$ nm pore
91   size (See Figure S1 in Supporting Information, SI).

92   NaOH, NaBr, NaCl salts were used as received. Fresh Milli-Q water was used throughout this work.
93   Experiments were carried out at room temperature T = 22 °C.

94   *Surface tension and sessile drop contact angle.* Surface tension was used to measure surfactant adsorption
95   on porous particles. All measurements were performed in a 9 cm diameter polystyrene Petri dish
96   containing a volume $V = 35$ mL of surfactant solutions at different concentrations C and a fixed mass (1.2
97   mg) of porous particles. For planar aqueous surfaces contained in a Petri dish, surface tension was
98   measured by the Wilhelmy plate method (KSV NIMA, Biolin Scientific) using a filer paper plate. In order
99   to evaluate the interfacial tensions of the silica-surfactant solutions-gas systems, we also measured the
100   surface tension of aqueous solutions and the advancing contact angle θ of sessile drops by a profile
101   analysis tensiometer (PAT, Sinterface, Germany). A typical volume of the aqueous drop in PAT
102   experiments is 15 mm^3. Series of experiments were repeated at least three times and show a good
103   reproducibility. For interfacial tension measurements, the standard deviations of the data obtained in
104   different experimental campaigns lay between 1 and 3 mN/m, which can be related to the experimental
105   protocols: particle deposition, aging of particle dispersions and surfactant solutions (*i.e.* maximum 5
106   days).

107   *Particle dispersion deposition.* The final chosen method adopted to deposit porous particles at the
108   interface is to drop 1 mL of a 1.2 mg/mL particle suspension on a tilted glass slide placed at the air-water
109   interface and let it slip.[29] Particle density at the interface can be calculated by counting the particle
110   number using optical microscopy. For all porous particle systems, we evaluated an average surface
111   coverage of 6.5±2 particles per mm^2 (if 1.2 mg of silica porous particles are added in the Petri dish). From
112   the latter value, one can estimate the ratio between the total number of particles N_{tot} and the ones trapped
113   at the surface N_s: $N_{tot}/N_s \approx 10^6$, which is very high, meaning that only few particles stay at the interface.
114   We have put many efforts to find protocols to increase the number of particles remaining at the air-
115   aqueous solution interface and try several methods. However, protocols involving spraying or the use of
116   additional volatile solvents were discarded since they do not allow the control of the particles numbers or
117   introduce additional sources of contamination and uncertainties. It is important to note that even if N_{tot}/N_s
118   $\approx 10^6$, the amount of particles at the interface is non-negligible for the adsorption of soluble surfactants,
119   which accumulate preferentially at the interface but they are also present in the bulk, see Figure S2 in SI.

120   *Particle contact angle by gel trapping.* We measured the particle contact angle of porous silica colloids
121   using a gel trapping technique.[30] Few microliters of a diluted solution of particles were added to a gelled
122   solution of Phytagel (CAS 71010-52-1, Sigma Aldrich) in a small container. After heating up the gel to
123   the liquid state, the particles get trapped at the interface. Going back to the room temperature, a UV-glue
124   was used to transfer the particles from the gel to the glue substrate. The contact angle was measured using

125 scanning electron microscopy images of the transferred particles on the solidified glue at their
126 complementary contact angle positions.

127 *Particle tracking.* Bright field optical microscopy was used for particle tracking. Experiments were
128 performed in an upright Leica optical microscope mounted on an anti-vibration table. Images of isolated
129 particles were recorded using a CMOS camera (Orca Flash 4.0, Hamamatsu) at rates of 80 or 100 frames
130 per second using objectives of different magnifications ($\times$63 and $\times$100). Tracking of the particle location
131 was done by an *IDL* routine or by using an image correlation-based approach (''Stat Tracker St.
132 Andrews'') implemented in Labview (National Instruments).

133 *Zeta potential and pH measurements.* We measured the zeta potential ζ (Zetasizer Nano ZS, Malvern
134 Instruments) and the pH of the particle dispersions in pure water or in the presence of surfactants. For
135 porous silica colloids dispersions, a pH = 6.4 was always measured in pure water.

136
137

138 **RESULTS AND DISCUSSION**

139 **Interfacial tensions of CTA$^+$Br$^-$ and CTA$^+$OH$^-$ at the liquid-gas and solid-liquid**
140 **interfaces**

141 We started characterizing the adsorption of CTA$^+$ surfactants on non-porous silica by evaluating the
142 interfacial tension between silica and the aqueous surfactant solutions, γ_{SL}. Young equation for a sessile
143 drop of aqueous surfactant solutions on a silica substrate in air reads:

144 $$\gamma_{SG} = \gamma_{SL} + \gamma_{LG}\cos\theta,\qquad\qquad\qquad\qquad\qquad (1)$$

145 where the subscripts S, L and G represent solid, liquid and gas respectively. One can evaluate γ_{SL}
146 measuring the interfacial tension γ_{LG}, the sessile drop static contact angle θ and assuming that γ_{SG} is a
147 constant (and does not vary with the surfactant concentration). Surface tension at the air-aqueous solution
148 interface γ_{LG} for CTA$^+$Br$^-$ and CTA$^+$OH$^-$ surfactant was measured by the Wilhelmy plate technique and
149 pendant drop tensiometry. The two methods lead to very similar results as shown for a series of
150 experiments in Figure 1A. The evolution of γ_{LG} as a function of the surfactant concentration C for both
151 surfactants shows no significant difference. In addition, γ_{LG} values are stable and do not change in a
152 typical experimental time range of 3000 s (inset of Figure 1A). Sessile drops made with surfactants
153 solutions were deposited on clean glass slides and their contact angles θ were also evaluated by imaging
154 the drop profile (and the $\cos\theta$ is plotted in the inset of Figure 1B for a series of experiment).[31] Hence, γ_{SL}
155 can be calculated from eq. 1 with γ_{SG} = 68.5 mN/m as reported by Binks et al.[32] for silica surfaces
156 showing water contact angle similar to our experiments. Unexpectedly the silica-aqueous solution
157 interfacial tension γ_{SL} shows a non-monotonic behavior if the surfactant concentration is increased.[33,34] For
158 $C \geq 0.1$ mM, γ_{SL} increases if C increases, instead of decreasing as γ_{LG}. Hence, the Gibbs adsorption valid
159 for ideal dilute solutions for C < CMC ($\approx$ 0.8-0.9 mM)[10,35] can be applied only for the air-liquid interface,
160 where a surface concentration $\Gamma \approx 1$ mg/m^2 at the CMC can be evaluated.[36] For C < 0.1 mM at the solid-
161 liquid interface, one could also observe a tiny decrease of the interfacial tension which could correspond
162 to an increasing accumulation of non-interacting surfactants at the solid-liquid interface.[37] However for C
163 ≥ 0.1 mM, the increase of γ_{SL} points to the formation of self-assembled structures as bilayers[38] or surface
164 micelles, which form because of the hydrophobic interactions between surfactant tails. Note that the

165 concentration at which the interfacial tension γ_{SL} increases is about 10 times lower that the CMC.[10] An
166 increase of the interfacial tension γ_{SL} reveals that the surface is increasing in hydrophobicity due to the
167 presence of hydrophobic surfactant groups. As already pointed out in the Introduction, the presence of
168 bilayers or surface micelles on planar silica surfaces has been widely reported but to the best of our
169 knowledge was never connected to a minimum in the interfacial tension γ_{SL}.
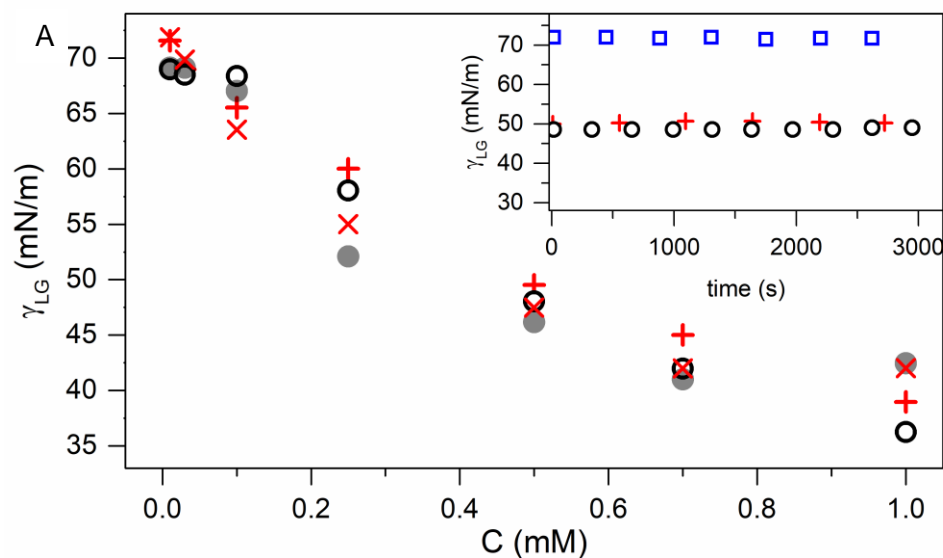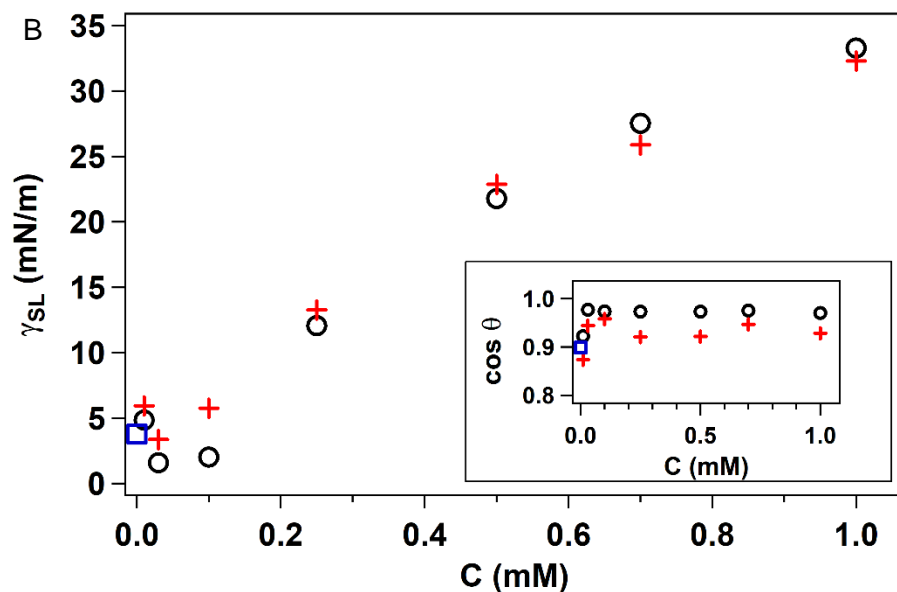
174 Figure 1. (A) Liquid-gas interfacial tension of CTA$^+$Br$^-$ (+, □) and CTA$^+$OH$^-$ (−, ｡) as a function of the
175 concentration obtained by pendant drop tensiometry (+,−) and by Wilhelmy plate method (□, ｡); inset: interfacial
176 tension as a function of time for pure water (∀) and CTA$^+$Br$^-$ (+) and CTA$^+$OH$^-$ (−) at $C = 0.5$ mM. (B) Solid-liquid

177 interfacial tension CTA$^+$Br$^-$ (+) and CTA$^+$OH$^-$ (−) evaluated by the Young equation and advancing contact angle
178 measurement of sessile drops on silica (inset). Data for pure water (∀) are also shown.

179

Porous particles at the interface

181 The contact angle of porous particles at the gas-liquid interface was measured by a gel trapping method
182 (see Materials and Methods). Figure 2 shows images of particles at their complementary contact angle
183 positions. We have also observed some crater shape footprints on the solidified substrate, which
184 correspond to particles possessing very low contact angles. For spherical porous particle, we measured
185 particle contact angle $\alpha = 47° \pm 6°$ for $d = 2$ nm and $\alpha = 52° \pm 14°$ for $d = 4$ nm (Figure 2A and B). Non-
186 spherical porous particles show also a finite immersion at the air-water interface that is comparable to the
187 contact angle observed for the spherical porous particles.
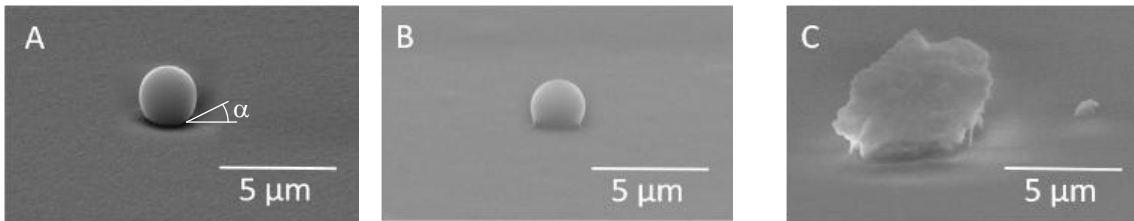
192 Figure 2. SEM images of gel trapped $\bar{R} = 1.23$ µm spherical mesoporous silica colloids $d = 2$ nm (A) and $d = 4$ nm
193 (B); and a non-spherical silica particle of equivalent radius $\bar{R} = 1.96$ µm (diameter = 3.92 µm) and $d = 7$ nm (C).

194

195 It is important to notice that the measured contact angle of a sessile water drop on silica, $\theta \approx 26°$, is
196 significantly lower than the contact angles of porous silica particles shown in Figure 2: $\alpha > \theta$. In order to
197 explain this result, we start discussing the partial wetting state of porous particles and compare it to the
198 reference case of a bare solid spherical particle, see Figure 3. For a bare particle, the equilibrium of
199 interfacial tensions leads to the Young equation (see equation 1). For smooth and homogenous surfaces,
200 the bare solid micron-sized particle contact angle should be identical to the contact angle of a sessile
201 liquid drop on a flat solid substrate: $\alpha_B = \theta$.[39] In the framework of the Cassie-Baxter model valid for
202 composite interfaces, two different scenario can be considered for porous particles at the interface.

203 In the first case, we consider that the pores of the particles are completely filled by the liquid. In this case,
204 the particle interfacial tensions γ_{SG} and γ_{SL} change if compared to the bare particle case. The interfacial
205 tension of the particle exposed to the liquid will be reduced from γ_{SL} to $f\gamma_{SL}$, where f is the solid area
206 fraction on the particle surface, see Figure 3. The particle surface exposed to the gas phase can be
207 regarded as a composite interface made of solid and liquid.[39] The resulting equilibrium of interfacial
208 tensions reads:

209 $f\gamma_{SG} + (1-f)\, \gamma_{LG} = f\gamma_{SL} + \gamma_{LG}\cos\alpha$.   (2)

210 Except for f, all the other variables in equation 2 are measured. In pure water, $\gamma_{SG} = 68.5$ mN/m, $\gamma_{LG} =$
211 72.5 mN/m and $\gamma_{SL} = 4$ mN/m (Figure 1). According to equation 2, α decreases if f decreases and the
212 Young equation is recovered if $f = 1$. Actually for porous particles with pores completely filled by the
213 liquid, the particle contact angle α is expected to be low, $\alpha < \theta$, which explains the observation of crater
214 footprints in SEM images and the large number of particles in the volume with respect to the particles
215 present at the interface (see Particle dispersion deposition section). Note also that the interfacial energy

6

216 gain associated to the adsorption of a bare particle at the interface $\gamma_{LG}A_0$ due to the removal of a bare fluid
217 interface area ($A_0 = \pi R^2 \sin^2\alpha$) is strongly reduced for a porous particle given the presence of liquid inside
218 the particle.[39]

219 A second scenario can be considered to explain the results shown in Figure 2, where $\alpha > \theta = \alpha_B$ (Figure
220 3). In this case, the liquid is not present on the porous particle surface exposed to the gas phase. Hence,
221 the external surface can be regarded as a composite surface made of solid and air, and the interfacial
222 tension of this surface becomes $f\gamma_{SG}$. The resulting equilibrium of interfacial tensions reads:

223 $f\gamma_{SG} = f\gamma_{SL} + \gamma_{LG}\cos\alpha$. (3)

224 In this second case, the contact angle of a porous particle can be higher than the contact angle of an
225 equivalent bare particles. Equation 3 can be rewritten in the form $\cos\alpha = \frac{f(\gamma_{SG}-\gamma_{SL})}{\gamma_{LG}} = f\cos\theta$ (see
226 equation 1), which leads to solid area fraction $f = 0.76$ for 2 nm and $f = 0.68$ for 4 nm pore size porous
227 particles.
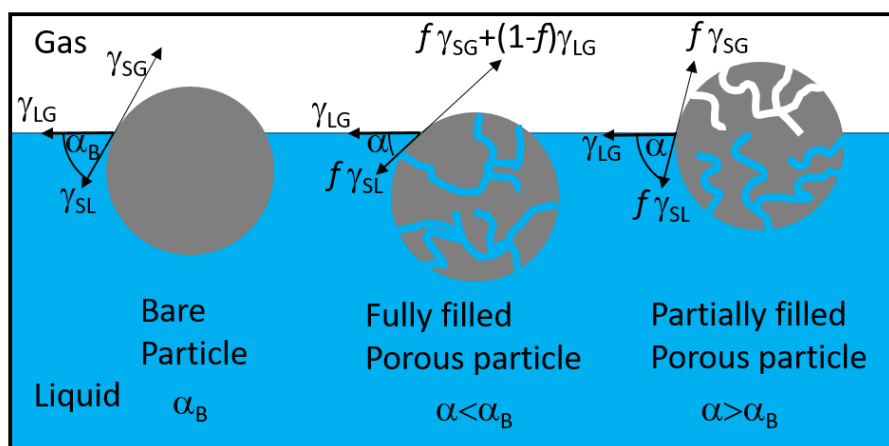
229 Figure 3. Sketches of a bare non-porous particle (left), a porous particle with pores completely filled by the liquid
230 (center) and a porous particle with pores partially filled by the liquid (right) in mechanical equilibrium at the gas-
231 liquid interface.

## Influence of particle pore size on surfactant adsorption

234 In order to measure the surfactant adsorption on porous silica colloids we performed surface tension
235 experiments using a Wilhelmy plate apparatus. Starting from a stable interfacial tension measurement at a
236 given surfactant concentration C, porous colloids are deposited at the air-aqueous solution interface via a
237 tilted glass slide. Note that the addition of few porous colloids (1.2 g in 35 mL water) in absence of
238 surfactants does not affect the interfacial tension γ_{LG}. As a consequence of the addition of mesoporous
239 particles, we record an increase of the liquid-gas interfacial tension connected to a surfactant removal
240 from the aqueous solution due to the adsorption on porous silica colloids.

241 In Figure 4 we show a series of surface tension experiments of CTA$^+$Br$^-$ and CTA$^+$OH$^-$ solutions at
242 different surfactant concentrations in the presence of a fixed number of porous silica particles of 4 and 7
243 nm pore diameters d. For CTA$^+$OH$^-$ in the presence of the $d = 4$ nm (Figure 4A) and 7 nm (Figure 4B)
244 porous silica particles, we measured a significant increase in the surface tension, which is a clear evidence

245 of surfactant removal from the aqueous solution. When adding $d = 4$ nm porous silica colloids, the
246 interfacial tension increases by 8 mN/m, 5 mN/m and 4 mN/m for 0.25 mM, 0.5 mM and 0.7 mM
247 respectively. As for the $d = 7$ nm porous silica colloids, the surface tension increases by 12 mN/m, 9
248 mN/m and 7 mN/m for 0.25 mM, 0.5 mM and 0.7 mM respectively. Surprisingly, no apparent increase in
249 the surface tension with CTA^+Br^- was observed, which will be further analyzed and discussed in the
250 following sections. No adsorption for both CTA^+Br^- and CTA^+OH^- was also observed for $d = 2$ nm
251 porous silica colloids, see Figure 5. Surface tension measurements showed no variation before and after
252 adding the $d = 2$ nm porous particles (Figure 5), leading to the conclusion that a pore size of 2 nm is too
253 small for CTA^+ cationic surfactant adsorption. This result agrees with the increase of γ_{SL} shown in Figure
254 1B and connected to the formation of surface micellar structures at concentrations much lower than the
255 CMC. Surfactants may adsorb inside the pores as micellar structures and not as single molecules. The size
256 of micelles in the bulk[10] (for $C \approx$ CMC) is between 2.6 and 4.7 nm; and for $C <$ CMC the thickness of
257 surface micelles is about 3.5 nm for CTA^+Br^-. Hence, these dimensions are always larger than the size of
258 2 nm and explain why adsorption is not observed in $d = 2$ nm porous particles.
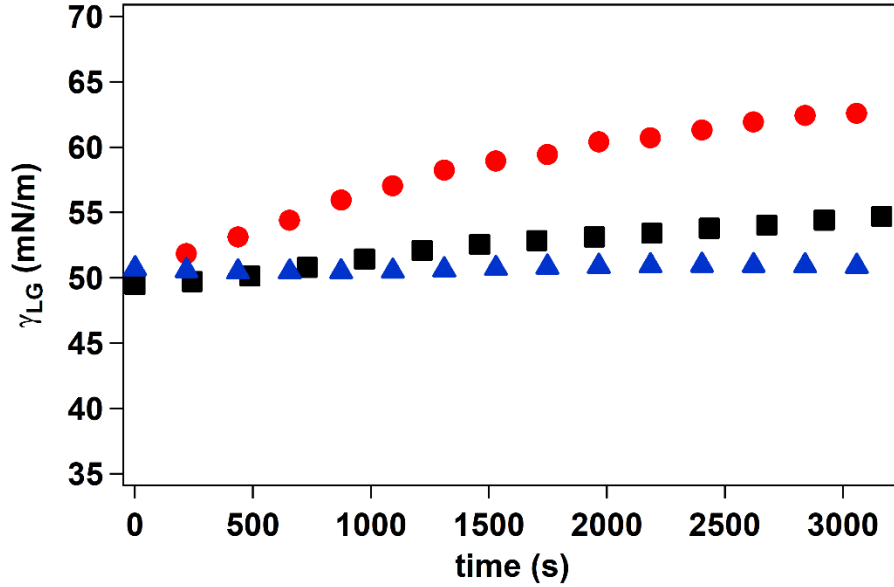
8

259

260
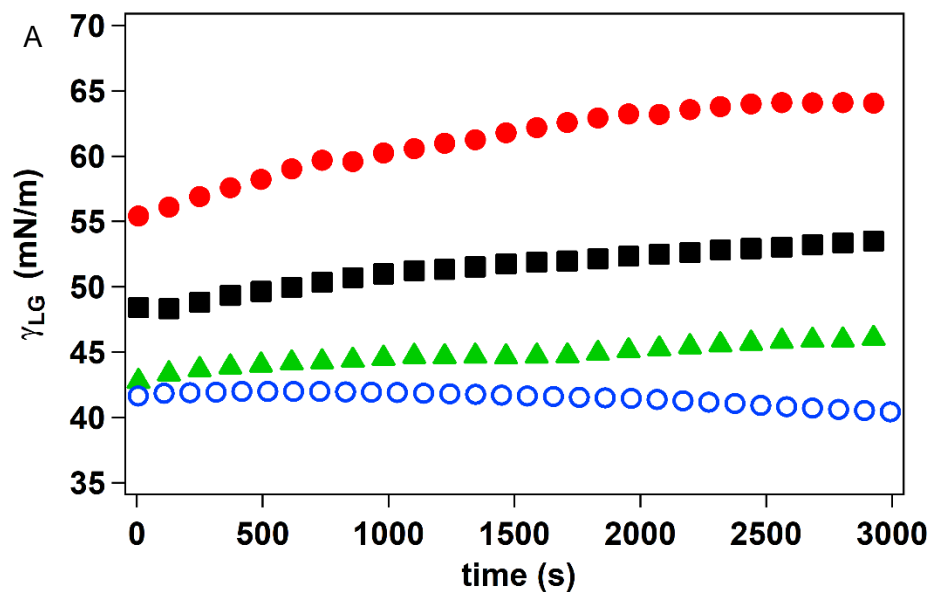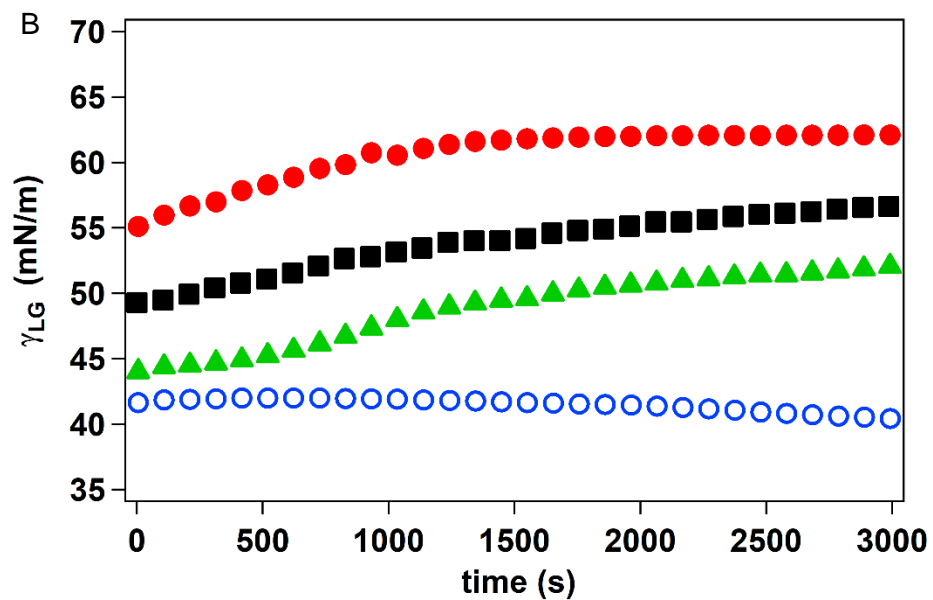
Figure 4. Liquid-gas interfacial tension as a function of time after the deposition of d = 4 nm porous silica particles (A) and d = 7 nm particles (B) at different CTA^+OH^- surfactant concentrations: C = 0.25 mM (,), 0.5 mM (!), 0,7 mM (7); and CTA^+Br^- concentration C= 0.7 mM (−). 1.2 g of particles were added in 35 mL solution.

265

Figure 5. Liquid-gas interfacial tension as a function of time for CTA$^+$OH$^-$ at $C = 0.5$ mM in the presence of $d = 7$ nm (●), $d = 4$ nm (■) and $d = 2$ nm (▲) porous silica particles (1.2 g of particles in 35 mL).

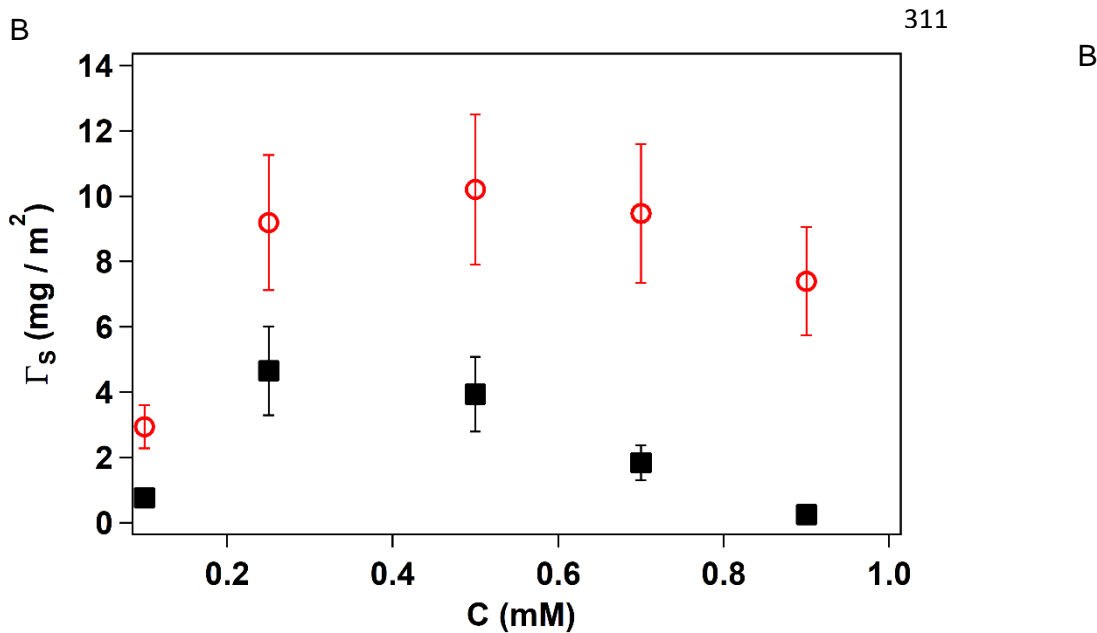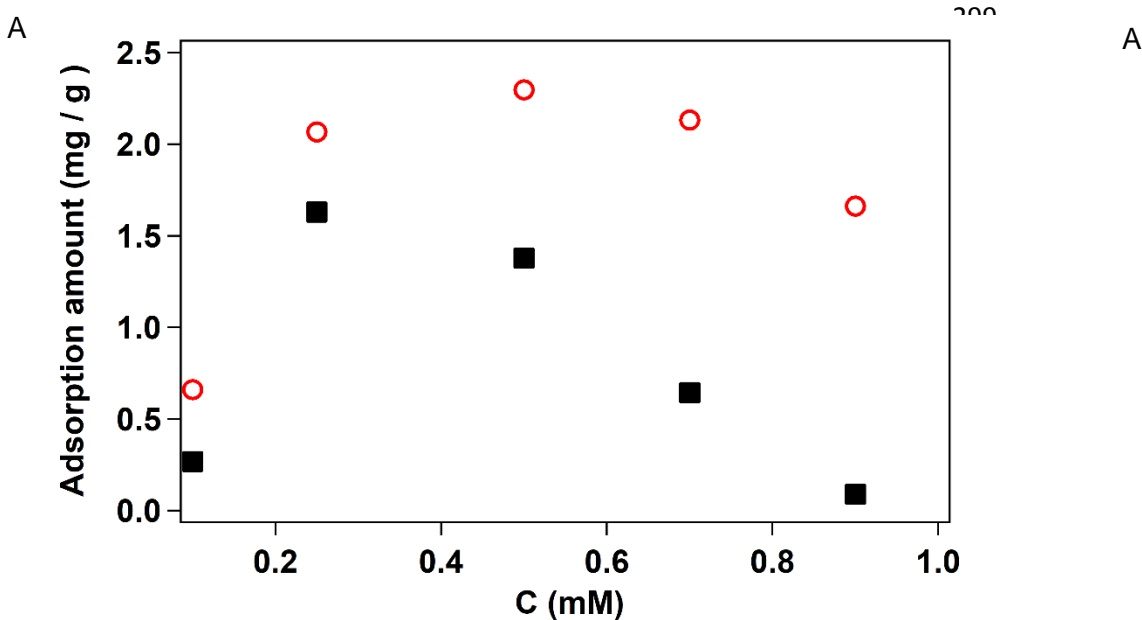Knowing the initial CTA$^+$OH$^-$ surfactant concentration C and the interfacial tension γ_{LG} after adsorption (at time $t = 3000$ s in Figure 4 and 5), we can extract the final surfactant concentration C_f in the solution using the γ_{LG} vs C data (eventually interpolated) shown in Figure 1A. Hence, we can calculate the total mass of surfactant removed in the $V = 35$ mL solution as $(C - C_f)V$. In Figure 6A, the adsorption amount (which is the mass of surfactants divided by the mass of porous particles) is plotted as a function of the initial surfactant concentration. For $d = 7$ nm porous silica particles, the adsorption amount increases up to 2 mg/g at intermediate concentrations. For $d = 4$ nm porous silica particles instead a maximum in the adsorption amount is clearly observed at $C = 0.25$ mM, above which the adsorption amount decreases. Knowing the mass m (=1.2 mg) of the porous particles and their specific areas S_A (see Materials and Methods), we can also calculate the surfactant surface concentration Γ_S on the total silica area (= mS_A):

$$\Gamma_S = \frac{(C - C_f)V}{m\, S_A} \tag{4}$$

Figure 6B shows Γ_S as a function of CTA$^+$OH$^-$ concentration for $d = 4$ and 7 nm porous silica particles. For $C = 0.1$ mM, we measured a weak adsorption of surfactants on porous silica particles $\Gamma_S = 1\text{-}3$ mg/m^2, which is equivalent to the surface excess of CTA$^+$ surfactant forming dense monolayers at the interface. For non-spherical silica particles with $d = 7$ nm, Γ_S increases up to 10 mg/m^2 at intermediate concentrations and slightly decreases if C approaches the CMC (≈ 0.9 mM). For spherical silica particles with $d = 4$ nm, the surface concentration increases up to $\Gamma_S \approx 4$ mg/m^2 and significantly decreases if C approaches the CMC. It is interesting to note that at low concentrations, Γ_S is proportional to the pore size, meaning that pores are filled with surfactants. In this pore size range and for surfactant concentrations far from the CMC, the larger the pore diameter the larger the surfactant adsorption. Close to the CMC however surfactants start to self-assemble in the form of micelles in the volume. As a consequence, a competition between the self-assembly of surfactants in the volume and the adsorption inside the pores of the silica particles is expected. This competition may also depend on the confinement

10

dictated by the pore size. If the pore confinement effect is very strong, micelles in the volume could hinder surfactant adsorption inside the particles' pores. For $d = 4$ nm porous particles, the decrease of Γ_S as a function of concentration seems in agreement with this scenario. For pore size $d = 7$ nm, the pore confinement effect is weaker than for $d = 4$ nm given that the micellar dimensions are about 3.5 nm, i.e. the half of the pore size, which explains the weak decrease of Γ_S as a function of concentration close to the CMC, see Figure 6B.

Porous particle diffusion at the gas-liquid interface

At the single colloidal particle level, we have also noticed striking differences in the translational diffusion of spherical $d = 4$ nm porous particle at the gas-liquid interface in the absence and the presence of CTA^+ surfactants. Tracking the particle center of mass at the air-water interface, we observed Brownian trajectories (see inset Figure 7A) and measured the mean squared displacement (MSD), which is plotted as a function of the lag time Δt in Figure 7A. Translational diffusion coefficients at the surface, D_s: can be calculated by $MSD = 4 D_s \Delta t$.

In absence of surfactants, D_s for $d = 2$ and 4 nm pore particles agrees with the hydrodynamic prediction for partially immersed particles at clean and flat fluid interface, see Figure 7B:[40]

$$D_S = \frac{k_B T}{k_t \eta R},$$ (5)

where $k_B T$ is the thermal agitation energy, η is the liquid viscosity and k_t is the drag factor accounting for the particle immersion or contact angle at the interface:[40]

$$k_t = 3\pi \left[1 + \frac{9}{16} \cos\alpha + \mathcal{O}(\cos^2\alpha) \right] \text{ (for } 0 < \alpha < 90°) .$$ (6)

For the particle diffusing in the bulk our experimental results agree with the Stokes-Brownian diffusion $D_0 = \frac{k_B T}{6\pi\eta R} = 0.174$ μm²/s. In absence of surfactants, the good agreement between the $1.4 < D_S/D_0 < 1.5$ experiments and the prediction shows that no additional dissipation due to contact line fluctuations (as observed for bare silica colloids with $1.2 < D_S/D_0 < 1.3$)[41] occur on partially wetted porous particles. As pointed out before the external porous particle surface can be regarded as a composite surface made of hydrophilic silica and fluids. Hence, this surface presents less defects than the surface of a bare particle, which may explain the negligible line friction due to surface defects.[41] As a perspective, one may wonder if these porous particles could be good probes for passive surface microrheology since the only sources of dissipations seem to be the viscosity.

Surface diffusion coefficients of porous particles change significantly in the presence of CTA^+OH^- ($C = 0.5$ mM): $1.1 < D_S/D_0 < 1.2$, and in CTA^+Br^- ($C = 0.5$ mM) aqueous solutions: $D_S/D_0 \approx 0.3$, see Figure 7. The experiments are performed at times ≈ 3000 s, where an increase of the gas-liquid interfacial tension of 5 mN/m for CTA^+OH^-; and no change for CTA^+Br^- were measured, see Figure 4. Hence the presence of surfactants affect strongly the porous particle translational diffusion at the surface. For porous particles in the presence of CTA^+OH^-, adsorption of surfactants inside the pores occurs during the porous particle Brownian motion, whilst in the presence of CTA^+Br^- no adsorption dynamics occurs. In order to quantify the decrease of the surface translational diffusion D_S, we use a model describing the drag felt by a spherical particle straddling a viscous and incompressible interface possessing a surface viscosity η_S at low Boussinesq numbers $B_0 = \frac{\eta_S}{\eta R} < 1$. The drag factor in equation 5 in this case reads:[42]

$$k_t = k_t^{(0)} + B_0 k_t^{(1)} + \mathcal{O}(B_0^2),$$ (7)

$$k_t^{(0)} \approx 6\pi\sqrt{\tanh[32(1 + \cos\alpha)/(9\pi^2)]}$$

$$k_t^{(1)} \approx -4\ln\left[\frac{2}{\pi} \arctan\left(\frac{(1+\cos\alpha)}{3} \right) \right]$$

360   For CTA^+Br^- (C = 0.5 mM) aqueous solutions, a surface viscosity $\eta_S \approx 10^{-8}$ Pa.s.m fits well the
361   experimental result. In the literature, a large range of values of η_S, from 10^{-8} to 10^{-6} Pa.s.m, are reported
362   for soluble monolayers by surface macrorheology.[43] Usually a large difference is also measured between
363   surface macro- and micro-rheology ($\eta_S = 10^{-10} \dots 10^{-9}$ Pa.s.m),[44] which could be due to additional
364   dissipations or some boundary conditions not included in the analysis of the results.[45,46] Recent
365   experiments using noncontact microrheology, with completely wetted particles as probes, report η_S
366    $\approx 10^{-8} \dots 10^{-7}$ Pa.s.m,[45] which agree with our results for CTA^+Br^-. For CTA^+OH^- instead our results $\eta_S \approx$
367   5.10^{-10} Pa.s.m are comparable to passive surface microrheology using partially wetted particles as probe
368   particles.[44] Given that the liquid-gas interfacial tensions are similar for CTA^+Br^- and CTA^+OH^-, one
369   possible explanation of the difference in D_S between the two surfactant solutions is related to the
370   surfactant dynamics occurring at the porous particle surface. As already pointed out before, the adsorption
371   of CTA^+OH^- surfactants inside the pores could lead to a local depletion of the surfactant concentration
372   close to the external surface of the porous particle and therefore in a smaller surface viscosity felt by the
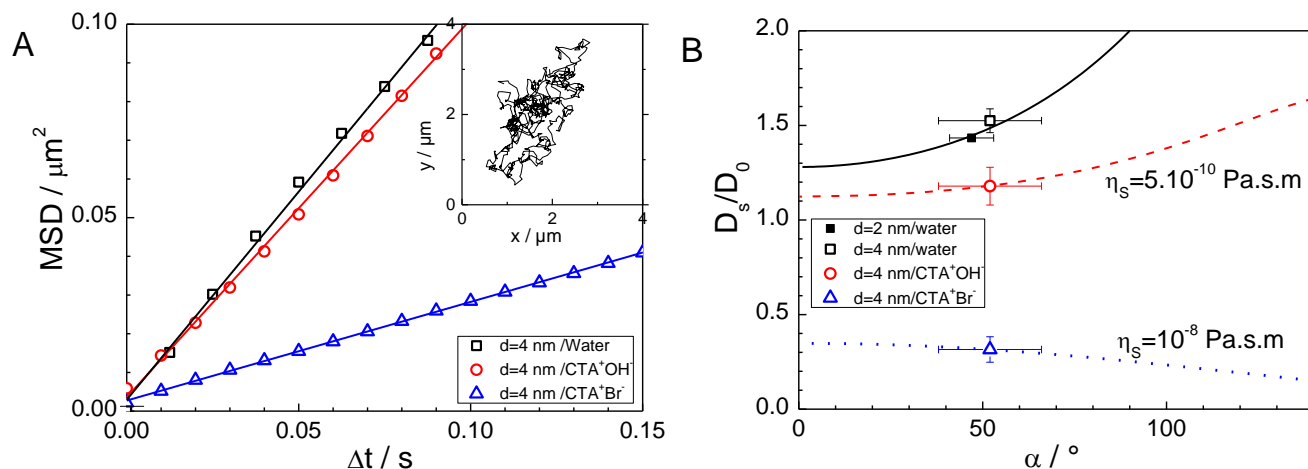
373   particle.

374

375   Figure 7. (A) Mean squared displacement as a function of the lag time for d = 4 nm porous particles at the gas-liquid
376   interface in pure water ($\forall$), in C = 0.5 mM CTA^+OH^- aqueous solution (−) and in C = 0.5 mM CTA^+Br^- aqueous
377   solution (8). The inset shows a typical particle Brownian trajectory at the surface. (B) Ratio between the surface and
378   the bulk diffusion coefficients as a function of the particle contact angle for the same systems shown in (A) and for d
379   = 2 nm porous particles at the gas-liquid interface in pure water (!). Solid line is the hydrodynamic prediction for a
380   bare and clean interface. Dashed and pointed lines are drawn from a model valid for viscous and incompressible
381   interfacial layers with a given surface viscosity η_S.

382

Influence of the counterion on surfactant adsorption

384   We start this section by analysing the remarkable difference in surfactant adsorption on porous particles
385   observed between CTA^+OH^- and CTA^+Br^-. For planar non-porous interfaces, both interfacial tensions at
386   the liquid-solid and liquid-gas point to a very similar behaviour for CTA^+ surfactants, independently from
387   the counterions. However, CTA^+Br^- surfactants do not adsorb on d = 4 and 7 nm porous particles, while

13

388 CTA^+OH^- surfactants adsorb with very high surface excess concentrations $\approx$ 4-10 mg/m^2 for C around 0.5
389 mM.

390 To explain this striking different behavior we started to look at the pH of the solution. Adding
391 CTA^+OH^- surfactants in the solution in fact alters the pH of water, which changes from 6.4 to 10.5 for C
392 = 0.5 mM. It is also well known that for planar silica surfaces, cationic surfactant adsorption usually
393 increases if the pH increases because of the increase negative charge of the silica surface.[35] In order to test
394 this hypothesis, we have added Na^+OH^- to a CTA^+Br^- solution (C = 0.5 mM) in the presence of porous
395 particles. The final pH measured is very similar (pH = 10.7) to the pH of CTA^+OH^- surfactants where a
396 strong adsorption was observed. However also in this case, CTA^+Br^- surfactants do not significantly
397 adsorb on porous silica particles, see Figure 8. It is also important to notice that for planar interfaces,
398 CTA^+Br^- adsorb on silica even if the pH remains around 6.[35]

399 If OH^- ions are not sufficient to trigger surfactant adsorption on porous particles, we consider the opposite
400 scenario for which the ion Br^- is able to hinder CTA^+ adsorption on silica. Therefore, in the presence of
401 porous particles, we measure the surface tension of CTA^+OH^- solution adding 1 mM of Na^+Br^-. In this
402 case, we observe that the surface tension of CTA^+OH^- (in the presence of porous particles) remains
403 constant instead of increasing, see Figure 8. Thus, it confirms that CTA^+ do not adsorb inside the pores of
404 d = 4 and 7 nm silica particles if Na^+Br^- is present in the aqueous solution.
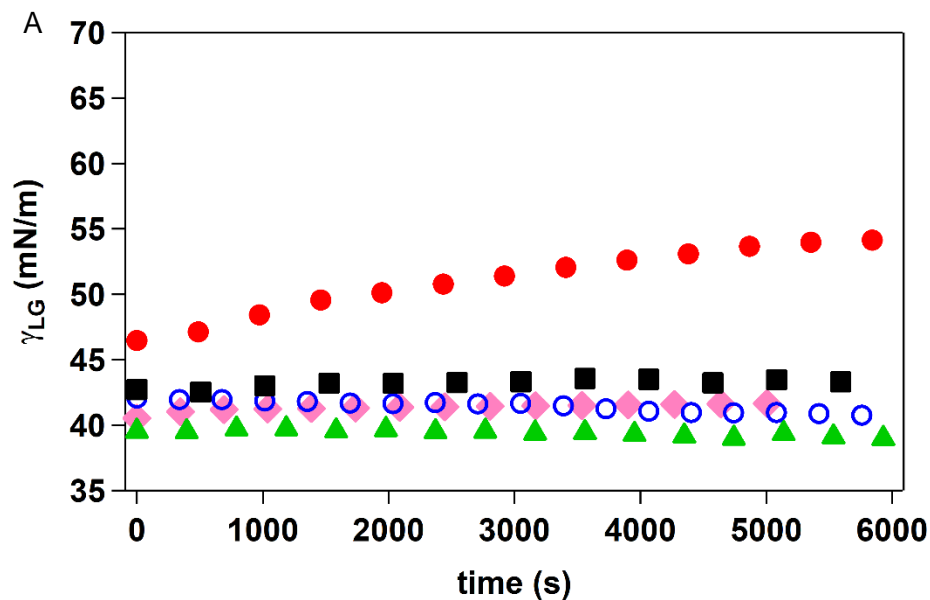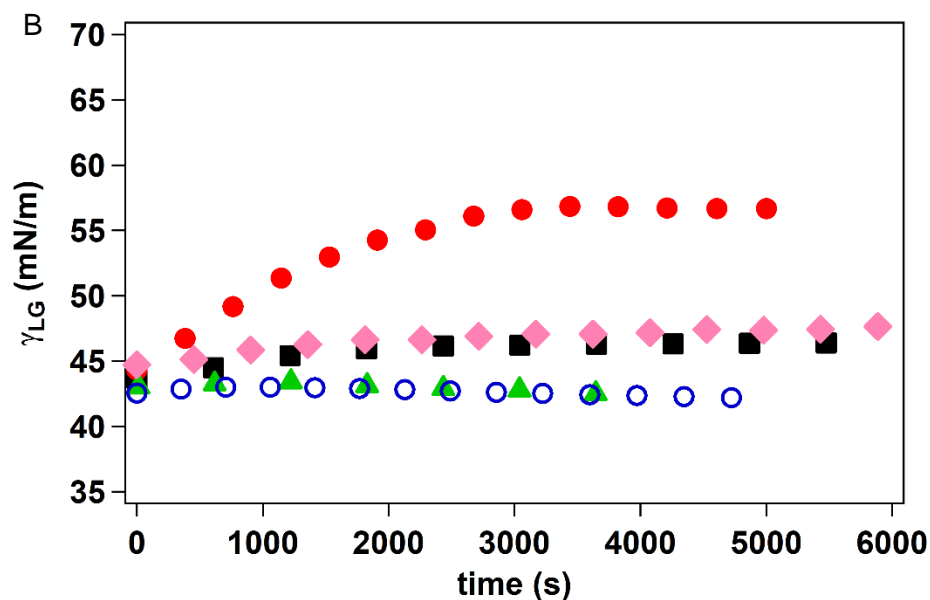
Figure 8. Salt effect on the liquid-gas interfacial tension as a function of time after porous particle deposition for $d = 4$ nm particles (A) and $d = 7$ nm particles (B). The surfactant concentration is fixed, $C = 0.5$ mM, CTA^+OH^- data (,) are the same as in Figure 2. Data for $CTA^+ Br^-$ + NaOH (!), CTA^+OH^- + [NaBr] = 1 mM (7), CTA^+OH^- + [NaCl] = 1 mM (Λ) and CTA^+Br^- + [NaCl] = 1 mM (−) as a function of time are also shown.

In order to verify if this effect is specific to Na^+Br^-, we have also tested another salt: Na^+Cl^-. The surface tension of CTA^+OH^- (in the presence of porous particles) in this case increases only by 1 to 3 mN/m, which confirms a salt hindrance effect on adsorption (see Figure 8).

Attempting to rationalize these finding, we consider some specific ionic phenomena related to adsorption phenomena. Some properties of OH^-, Br^-, Cl^- and Na^+ are listed in table 1.The main differences between the three negative ions are their hydration numbers (3 for OH^-, 2 for Cl^- and just 1 for Br^-) and their

15

418 Jones-Dole viscosity B coefficients connected to their ability to weaken or strengthen the interfacial water
419 structure close to hydrophobic molecules such as the surfactant tails. Cl^- is at the border ($B \approx 0$ M^{-1})
420 between chaotropic Br^- ($B = -0.04$ M^{-1}) and kosmotropic OH^- ($B = +0.18$ M^{-1}) behaviors.[47] Hence OH^-
421 may favor hydrophobic interactions between CTA^+ hydrophobic groups, which supports the adsorption of
422 surface micelles; whereas Br^- leads to a weakening of these hydrophobic interactions. We have also
423 measured the zeta potential ζ on bare porous particles,[48,49] which shows always negative values: $\zeta = -28.5$
424 mV for $d = 4$ nm and $\zeta = -7.8$ mV for $d = 7$ nm; as expected for hydrophilic silica.[50] For CTA^+OH^-
425 surfactants, ζ remains negative for $C = 0.25$ mM: $\zeta = -19.5$ mV for $d = 4$ nm and $\zeta = -7.8$ mV for $d = 7$
426 nm particles. On the contrary, in the presence of CTA^+Br^-, positive zeta potentials were measured at the
427 same concentration ($C = 0.25$ mM): $\zeta = +5.3$ mV for $d = 4$ nm and $\zeta = +5.9$ mV for $d = 7$ nm particles,
428 which points to the accumulation of positive charges on the external surface of the porous silica colloids.
429 Hence, CTA^+ from CTA^+Br^- (or H_3O^+) may accumulate on the silica portion of the porous particle outer
430 surface. This outer silica surface is very small with respect to the total porous particle surface, which may
431 explain the negligible change of the interfacial tension (or pH) observed in the experiments. Both the
432 chaotropic effect of Br^- and the repulsion due to the positive ζ lead to a hindrance of CTA^+ adsorption
433 inside the pores, which could explain the weak adsorption of CTA^+Br^- surfactants on porous silica
434 colloids.

435 Some additional specific ion effects occur on the surface of silica, where silanol groups are known to
436 undergo ion exchange reaction:[50,51] $X^+ + SiOH = X(SiO) + H^+$ for pH < 8, where X^+ is a cation (H_3O^+,
437 Na^+ or CTA^+), and for pH > 8, $SiOH + OH^- = SiO^-$. Hence a competition between H_3O^+, Na^+ or CTA^+
438 cations is also expected. Na^+ from Na^+Br^- and Na^+Cl^- in fact competes with CTA^+ in the adsorption on
439 silica,[52] which can explain the weakening of CTA^+OH^- adsorption in the presence of a sodium salt (see
440 Figure 8). Note that similarly to OH^-, Na^+ possesses an elevated hydration number and a positive B
441 coefficient corresponding to a kosmotropic behavior, see Table 1.

442

	OH^-	Br^-	Cl^-	Na^+
Bare ion radius (nm)[53]	0.176	0.195	0.181	0.095
Hydrated radius (nm)[53]	0.3	0.33	0.291	0.36
Hydration number (+/−1)[53]	3	1	2	4-5
B (M^{-1})[47]	+0.18	−0.04	−0.01	+0.06

443 Table 1

444

445

CONCLUSIONS

447 We have herein reported some fundamental aspects of the wetting and surface diffusion of porous
448 particles at the liquid-gas interface and explored the mechanisms underlying cationic surfactant
449 adsorption inside the particle's pores. Contact angle of porous particles at the gas-liquid interface can be
450 described in the framework of the Cassie model in partial wetting, and it depends strongly on the presence
451 of the liquid inside the pores of the particle. For pores completely filled by the liquid, the particle contact
452 angle is expected to be very low and porous particles may detach from the interface and diffuse in the
453 bulk. Particle translational diffusion at the pure water interface agrees with the hydrodynamics prediction,

which makes these particles ideal probes for interfacial microrheology. Porous silica colloids are already able to adsorb efficiently CTA^+OH^- surfactants without any chemical surface treatments on silica. We determined a significant adsorption of CTA^+OH^- surfactant on $d = 4$ and 7 nm pore size colloids. The lack of adsorption for $d = 2$ nm porous particles agrees with the presence of surface micelles and not monolayers of surfactants inside the pores of silica. We quantified CTA^+OH^- surface concentration and showed that for $C <$ CMC, the adsorption increases with the pore size. Therefore, we investigated the effect of the counterion on surfactant removal in order to understand the opposite adsorption behaviour observed between CTA^+OH^- and CTA^+Br^- on porous silica colloids. pH and surface charge effects are not able alone to explain our experimental findings, which points to the importance of kosmotropic/chaotropic counterion character. Surfactant adsorption on the porous particle affects also the particle translational diffusion at the interface, which points to different boundary conditions on the particle external surface.

Finally, these results can be used to implement an environmental friendly strategy to remediate the surface of water from soluble and insoluble pollutants. Yet for future investigations, we plan to functionalize porous silica particles with hydrophobic groups to target contaminants that accumulate preferentially only on the water surface. Moreover, based on our expertise on self-propelled Janus silica particles at the interface,[54,55] we plan to investigate the role of enhanced active diffusion on the kinetic of surfactant removal.[56] Attention will be paid to the effect of ionic species present in the aqueous medium on the self-propulsion particle behavior.[57,58]

ASSOCIATED CONTENTS

Supporting information

Non-spherical mesoporous silica particles pore size distribution, Particle deposition protocols.

References

(1)   Heinz, H.; Pramanik, C.; Heinz, O.; Ding, Y.; Mishra, R. K.; Marchon, D.; Flatt, R. J.; Estrela-lopis, I.; Llop, J.; Moya, S.; et al. Nanoparticle Decoration with Surfactants : Molecular Interactions , Assembly , and Applications. *Surf. Sci. Rep.* **2017**, *72* (1), 1–58.

(2)   Paria, S.; Khilar, K. C. A Review on Experimental Studies of Surfactant Adsorption at the Hydrophilic Solid – Water Interface. *Adv. Colloid Interface Sci.* **2004**, *110*, 75–95.

(3)   Olkowska, E.; Ruman, M.; Polkowska, Z. Occurrence of Surface Active Agents in the Environment. *J. Anal. Methods Chem.* **2014**, *2014*, 769708.

(4)   Li, Z.; Bowman, R. S. Counterion Effects on the Sorption of Cationic Surfactant and Chromate on Natural Clinoptilolite. *Environ. Sci. Technol.* **1997**, *31* (8), 2407–2412.

(5)   Kotti, M.; Papafilippaki, A.; Prassa, P.; Xirouhaki, A. Removal of Cationic Surfactants from Water by Adsorption on Attapulgite. *Comput. Water, Energy, Environ. Eng.* **2018**, *07* (03), 111–118.

(6)   Maria-Hormigos, R.; Pacheco, M.; Jurado-Sánchez, B.; Escarpa, A. Carbon Nanotubes-Ferrite-Manganese Dioxide Micromotors for Advanced Oxidation Processes in Water Treatment. *Environ. Sci. Nano* **2018**, *5* (12), 2993–3003.

(7)   Das, S.; Chakraborty, J.; Chatterjee, S.; Kumar, H. Prospects of Biosynthesized Nanomaterials for the Remediation of Organic and Inorganic Environmental Contaminants. *Environ. Sci. Nano* **2018**, *5* (12), 2784–2808.

(8)   Yang, K.; Wang, J.; Chen, X.; Zhao, Q.; Ghaffar, A.; Chen, B. Application of Graphene-Based Materials in Water Purification: From the Nanoscale to Specific Devices. *Environ. Sci. Nano* **2018**, *5* (6), 1264–1297.

(9)   Goloub, T. P.; Koopal, L. K.; Bijsterbosch, B. H.; Sidorova, M. P. Adsorption of Cationic Surfactants on Silica . Surface Charge Effects. *Langmuir* **1996**, *7463* (8), 3188–3194.

(10)   Atkin, R.; Craig, V. S. J.; Wanless, E. J.; Biggs, S. Mechanism of Cationic Surfactant Adsorption at the Solid – Aqueous Interface. *Adv. Colloid Interface Sci.* **2003**, *103* (03), 219–304.

(11)   Rennie, A.; Lee, E.; Simister, E.; Thomas, R. Structure of Cationic Surfactant Layer at the Silica-Water Interface. *Langmuir* **1990**, *6*, 1031–1034.

(12)   Tyrode, E.; Rutland, M. W.; Bain, C. D. Adsorption of CTAB on Hydrophilic Silica Studied by Linear and Nonlinear Optical Spectroscopy. *J. Am. Chem. Soc.* **2008**, *130* (51), 17434–17445.

(13)   Atkin, R.; Craig, V. S. J.; Biggs, S. Adsorption Kinetics and Structural Arrangements of Cationic Surfactants on Silica Surfaces. *Langmuir* **2000**, *16* (8), 9374–9380.

(14)   Biswas, S. C.; Chattoraj, D. K. Kinetics of Adsorption of Cationic Surfactants at Silica-Water Interface. *J. Colloid Interface Sci.* **1998**, *20* (205), 12–20.

(15)   Wangchareansak, T.; Keniry, M. A.; Liu, G.; Craig, V. S. J. Coadsorption of Low-Molecular Weight Aromatic and Aliphatic Alcohols and Acids with the Cationic Surfactant, CTAB, on Silica Surfaces. *Langmuir* **2014**, *30*, 6704–6712.

(16)   Lehman, S. E.; Larsen, S. C. Zeolite and Mesoporous Silica Nanomaterials: Greener Syntheses, Environmental Applications and Biological Toxicity. *Environ. Sci. Nano* **2014**, *1* (3), 200–213.
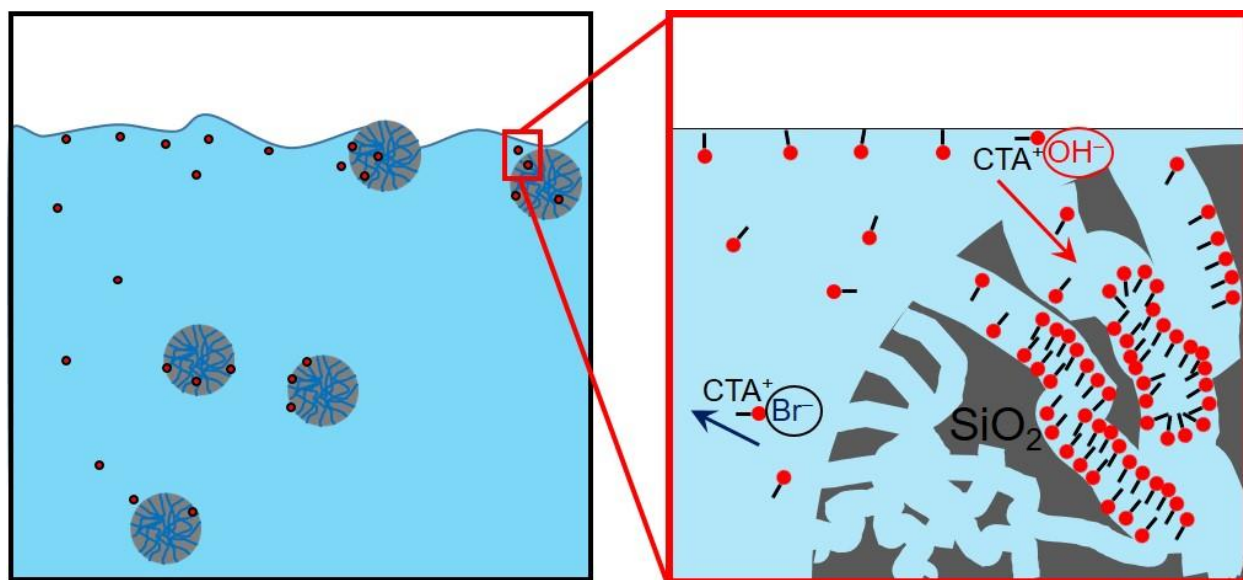
526 (17) Tang, Z.; Wang, J.; Zhao, T.; Shi, J.; Wu, F.; Giesy, J. P.; Zhang, H.; Zhao, X. Efficient Removal
527   of Both Antimonite (Sb(Iii)) and Antimonate (Sb(v)) from Environmental Water Using Titanate
528   Nanotubes and Nanoparticles. *Environ. Sci. Nano* **2019**, *6*, 834–850.

529 (18) Liu, L.; Yang, X.; Xu, Z.; Liu, L.; Yang, X.; Xu, Z. Gibbs Ensemble Monte Carlo Simulation of
530   Adsorption for Model Surfactant Solution in Confined Slit Pores. *J. Chem. Phys.* **2008**, *128*,
531   184712.

532 (19) Shin, T.; Dem, B.; Fratzl, P.; Paris, O.; Findenegg, G. H. Surfactant Self-Assembly in Cylindrical
533   Silica Nanopores. *J. Phys. Chem. Lett.* **2010**, *1*, 1442–1446.

534 (20) Shin, T. G.; Dirk, M.; Meissner, J.; Paris, O.; Findenegg, G. H. Structural Characterization of
535   Surfactant Aggregates Adsorbed in Cylindrical Silica Nanopores. *Langmuir* **2011**, *27*, 5252–5263.

536 (21) Qiao, Y.; Scho, M.; Findenegg, G. H. 2H NMR Investigation of the Structure and Dynamics of the
537   Nonionic Surfactant C12E5 Confined in Controlled Pore Glass. *Langmuir* **2003**, *19* (3), 6160–
538   6167.

539 (22) Müter, D.; Rother, G.; Bock, H.; Schoen, M.; Findenegg, G. H. Adsorption and Depletion
540   Regimes of a Nonionic Surfactant in Hydrophilic Mesopores : An Experimental and Simulation
541   Study. *Langmuir* **2017**, *33*, 11406–11416.

542 (23) Shin, T.; Findenegg, G. H.; Brandt, A. Surfactant Adsorption in Ordered Mesoporous Silica
543   Studied by SANS. *Prog. Colloid Polym. Sci.* **2006**, *133* (May), 116–122.

544 (24) Kumar, S.; Aswal, V. K.; Kohlbrecher, J. Size-Dependent Interaction of Silica Nanoparticles with
545   Different Surfactants in Aqueous Solution. *Langmuir* **2012**, *28*, 9288–9297.

546 (25) Sharma, K. P.; Aswal, V. K.; Kumaraswamy, G. Adsorption of Nonionic Surfactant on Silica
547   Nanoparticles : Structure and Resultant Interparticle Interactions. *J. Phys. Chem. B* **2010**, *114*,
548   10986–10994.

549 (26) Ahualli, S.; Iglesias, G. R.; Wachter, W.; Dulle, M.; Minami, D.; Glatter, O. Adsorption of
550   Anionic and Cationic Surfactants on Anionic Colloids : Supercharging and Destabilization.
551   *Langmuir* **2011**, *27*, 9182–9192.

552 (27) Tsubaki, J.; Jimbo, G. A Proposed New Characterization of Particle Shape and Its Application.
553   *Powder Technol.* **1979**, *22* (2), 161–169.

554 (28) Mouawia, R.; Mehdi, A.; Reyé, C.; Corriu, R. J. P. From Simple Molecules to Highly
555   Functionalised Lamellar Materials. *J. Mater. Chem.* **2008**, *18* (17), 2028–2035.
556   https://doi.org/10.1039/b719162f.

557 (29) Lotito, V.; Zambelli, T. Self-Assembly of Single-Sized and Binary Colloidal Particles at
558   Air/Water Interface by Surface Confinement and Water Discharge. *Langmuir* **2016**, *32* (37),
559   9582–9590.

560 (30) Paunov, V. N. Novel Method for Determining the Three-Phase Contact Angle of Colloid Particles
561   Adsorbed at Air - Water and Oil - Water Interfaces. *Langmuir* **2003**, *19* (13), 7970–7976.

562 (31) Zorin, Z.; Churaev, N.; Esipova, N.; Sergeeva, I.; Sobolev, V.; Gasanov, E. Influence of Cationic
563   Surfactant on the Surface Charge of Silica and on the Stability of Aqueous Wetting Films. *J.
564   Colloid Interface Sci.* **1992**, *152* (1), 170–182.

565 (32) Binks, B. P. Solid Wettability from Surface Energy Components: Revelance to Pickering
566   Emulsion. *Langmuir* **2002**, *18* (1), 1270–1273.

567 (33) Haidara, H.; Owen, M. J. A Direct Method of Studying Adsorption of a Surfactant at Solid-Liquid
568   Interfaces. *J. Phys. Chem.* **1995**, *99*, 8681–8683.

569 (34) Haidara, H.; Vonna, L.; Schultz, J. Kinetics and Thermodynamics of Surfactant Adsorption at
570   Model Interfaces : Evidence of Structural Transitions in the Adsorbed Films. *Langmuir* **1996**, *79*
571   (8), 3351–3355.

572 (35) Monticone, V.; Treiner, C. Coadsorption of Phenoxyalchohols and Cationic Surfactans with
573   Various Headgroups at the Silica/Water Interface. *J. Colloid Interface Sci.* **1994**, *166*, 394–403.

574 (36) Stocco, A.; Carriere, D.; Cottat, M.; Langevin, D. Interfacial Behavior of Catanionic Surfactants.
575   *Langmuir* **2010**, *26* (13), 10663–10669.

576 (37) Pyter, R. A. Wetting of Solids by Surface-Active Agents : The Effects of Unequal Adsorption to
577   Vapor-Liquid and Solid-Liquid Interfaces. *J. Colloid Interface Sci.* **1982**, *89* (1), 144.

578 (38) Rutland, M. W.; Parker, J. L. Surface Forces between Silica Surfaces in Cationic Surfactant
579   Solutions : Adsorption and Bilayer Formation at Normal and High PH. *Langmuir* **1994**, *10* (7),
580   1110–1121.

581 (39) Stocco, A.; Nobili, M. A Comparison between Liquid Drops and Solid Particles in Partial Wetting.
582   *Adv. Colloid Interface Sci.* **2017**, *247*, 223–233.

583 (40) Aaron, D.; Hardt, S. Drag and Diffusion Coefficients of a Spherical Particle Attached to a Fluid
584   Interface. *J. Fluid Mech.* **2015**, 1–11.

585 (41) Boniello, G.; Blanc, C.; Fedorenko, D.; Medfai, M.; Mbarek, N. Ben; In, M.; Gross, M.; Stocco,
586   A.; Nobili, M. Brownian Diffusion of a Partially Wetted Colloid. *Nat. Mater.* **2015**, *14* (9), 908–
587   911.

588 (42) Fischer, T. M.; Dhar, P.; Heinig, P. The Viscous Drag of Spheres and Filaments Moving in
589   Membranes or Monolayers. *J. Fluid Mech.* **2006**, *558*, 451.

590 (43) Langevin, D. Surface Shear Rheology of Monolayers at the Surface of Water. *Adv. Colloid
591   Interface Sci.* **2014**, *207*, 121–130.

592 (44) Sickert, M.; Rondelez, F.; Stone, H. a. Single-Particle Brownian Dynamics for Characterizing the
593   Rheology of Fluid Langmuir Monolayers. *Europhys. Lett.* **2007**, *79* (6), 66005.

594 (45) Shlomovitz, R.; Evans, A. A.; Boatwright, T.; Dennin, M.; Levine, A. J. Measurement of
595   Monolayer Viscosity Using Noncontact Microrheology. *Phys. Rev. Lett.* **2013**, *110* (13), 29–33.

596 (46) Stocco, A.; Chollet, B.; Wang, X.; Blanc, C.; Nobili, M. Rotational Diffusion of Partially Wetted
597   Colloids at Fluid Interfaces. *J. Colloid Interface Sci.* **2019**, *542*, 363–369.

598 (47) Marcus, Y. Effect of Ions on the Structure of Water. *Pure Appl. Chem.* **2010**, *82* (10), 1889–1899.

599 (48) Kozak, M. W.; Davis, E. J. Electrokinetics of Concentrated Suspensions and Porous Media. 1.
600   Thin Electrical Double Layers. *J. Colloid Interface Sci.* **1989**, *127* (1), 497–510.

601 (49) Kozak, M. W.; Davis, E. J. Electrokinetics of Concentrated Suspensions and Porous Media. 2
602   Moderately Thick Electrical Double Layers. *J. Colloid Interface Sci.* **1989**, *129* (1), 166–174.

603 (50) Allen, L. H.; Matijevic, E. Stability of Colloidal Silica. II Ion Exchange. *J. Colloid Interface Sci.*
604   **1970**, *33*, 420–429.

605 (51) Wängnerud, P.; Olofsson, G. Adsorption Isotherms for Cationic Surfactants on Silica Determined

606   by in Situ Ellipsometry. *J. Colloid Interface Sci.* **1992**, *153* (2), 392–398.

607 (52)   Dimov, N. K.; Kolev, V. L.; Kralchevsky, P. A.; Lyutov, L. G.; Broze, G.; Mehreteab, A.
608   Adsorption of Ionic Surfactants on Solid Particles Determined by Zeta-Potential Measurements :
609   Competitive Binding of Counterions. *J. Colloid Interface Sci.* **2002**, *256*, 23–32.

610 (53)   Israelachvili, J. N. *Intermolecular and Surface Forces*; Academic Press, 2011.

611 (54)   Wang, X.; In, M.; Blanc, C.; Nobili, M.; Stocco, A. Enhanced Active Motion of Janus Colloids at
612   the Water Surface. *Soft Matter* **2015**, *11*, 7376–7384.

613 (55)   Wang, X.; In, M.; Blanc, C.; Würger, A.; Nobili, M.; Stocco, A. Janus Colloids Actively Rotating
614   on the Surface of Water. *Langmuir* **2017**, *33* (48), 13766–13773.

615 (56)   Safdar, M.; Simmchen, J.; Jänis, J. Light-Driven Micro- and Nanomotors for Environmental
616   Remediation. *Environ. Sci. Nano* **2017**, *4* (8), 1602–1616.

617 (57)   Uygun, D. A.; Jurado-Sánchez, B.; Uygun, M.; Wang, J. Self-Propelled Chelation Platforms for
618   Efficient Removal of Toxic Metals. *Environ. Sci. Nano* **2016**, *3* (3), 559–566.

619 (58)   Eskandarloo, H.; Kierulf, A.; Abbaspourrad, A. Nano- and Micromotors for Cleaning Polluted
620   Waters: Focused Review on Pollutant Removal Mechanisms. *Nanoscale* **2017**, *9* (37), 13850–
621   13863.

622

623

624 TOC graphic

625

626